
# Natural Dextran as an Efficient Interfacial Passivator for ZnO-Based Electron-Transport Layers in Inverted Organic Solar Cells

ADVANCED ENERGY MATERIALS
www.advenergymat.de

# Natural Dextran as an Efficient Interfacial Passivator for ZnO-Based Electron-Transport Layers in Inverted Organic Solar Cells

*Bin Zhang,* Zhenshen Pan, Wenming Li, Yushou Zhao, Xiaolan Qin, Aiqin Li, Menglan Lv,* Xiaofeng Qin, Weile Guo, Zhicai He, and Ergang Wang**

**Compared to conventional organic solar cells (OSCs) with acidic PEDOT:PSS as the hole transport layer (HTL), inverted OSCs (i-OSCs) with zinc oxide (ZnO) as the electron transport layer (ETL) display significant advantages in terms of high stability. However, an obvious limitation in i-OSCs is that the sol-gel processed ZnO layers possess detrimental defects at the interface, which hinders the improvement of its photovoltaic performance. To address this problem, a natural, and green dextran (Dex) is used as an efficient interfacial passivator to modify the ZnO layer, thereby achieving enhanced device performance in i-OSCs. The introduction of the Dex passivator efficiently suppresses the interfacial recombination loss, resulting in higher power conversion efficiencies (PCEs). Interestingly, Dex-passivated ZnO exhibits broad applications as an ETL for different types of i-OSCs, including fullerene, non-fullerene, and all-polymer OSCs, in which the D18:Y6 system gives the highest PCE of 18.32%. This is one of the highest values reported for binary i-OSCs. Moreover, the application of Dex significantly improves the device stability, and the $T_{80}$ lifetimes based on PM6:Y6, D18:Y6, and PM6:PY-IT exceed 1500 h. These results imply that Dex is an excellent interfacial passivator for ZnO-based ETL for high-efficiency and stable i-OSCs.**

## 1. Introduction

Organic solar cells (OSCs) have attracted much academic and industrial interest owing to their distinct advantages of light weight, flexibility, feasible functionalization, and low-cost roll-to-roll fabrication.[1] Recently, owing to material design and device engineering, the power conversion efficiencies (PCEs) have exceeded 20% in both single-junction[2,3] and tandem OSCs.[4] This improvement indicates that OSCs exhibit extraordinary potential as competitive candidates for emerging energy technologies.

Most of these high-efficiency OSCs are based on the conventional ITO/PEDOT:PSS/active layer/cathode interfacial layer-(CIL)/cathode structure, where PEDOT:PSS is commonly used as the hole transport layer (HTL).[5–7] It has been established that PEDOT:PSS is an excellent HTL in OSCs because of its advantages in high conductivity and hole mobility, considerable optical transparency, and feasible solution processibility.[8,9] However, PEDOT:PSS also has shortcomings, especially the erosion of the ITO anode, which is detrimental for the realization of high stability in OSCs.[10–13] Therefore, there is an urgent need to develop alternative methods to overcome these problems, such as designing new HTL or developing new device architectures.

B. Zhang, W. Li, Y. Zhao, X. Qin, A. Li, M. Lv, X. Qin, W. Guo
Engineering Research Center for Energy Conversion and Storage Technology of Guizhou
School of Chemistry and Chemical Engineering
Guizhou University
Guiyang 550025, China
E-mail: zhangb@gzu.edu.cn; mllv@gzu.edu.cn

Z. Pan
Jiangsu Engineering Laboratory of Light-Electricity-Heat Energy-Converting Materials and Applications
School of Materials Science and Engineering
Changzhou University
Changzhou 213164, China

Z. He
Institute of Polymer Optoelectronic Materials and Devices
State Key Laboratory of Luminescent Materials and Devices
South China University of Technology
Guangzhou 510640, China

E. Wang
Department of Chemistry and Chemical Engineering
Chalmers University of Technology
Göteborg SE-412 96, Sweden
E-mail: ergang@chalmers.se

The ORCID identification number(s) for the author(s) of this article can be found under https://doi.org/10.1002/aenm.202404297



**DOI: 10.1002/aenm.202404297**

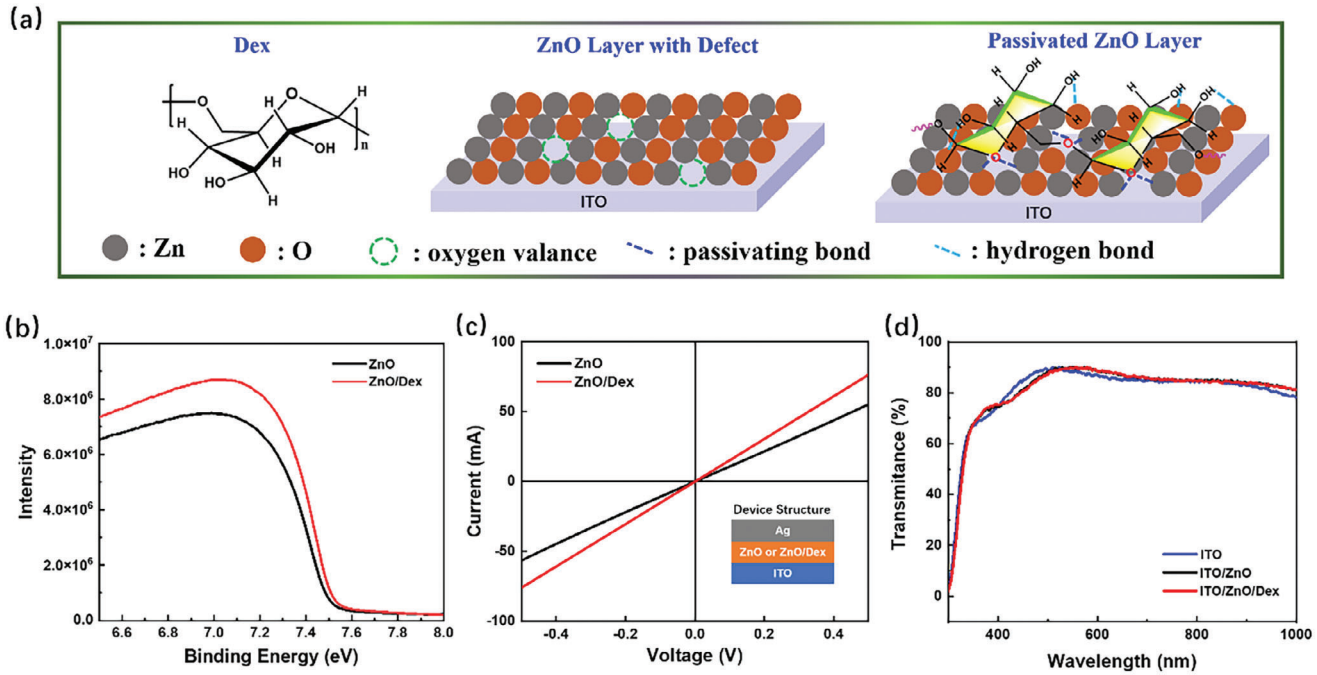


**Figure 1.** a) Proposed passivating mechanism with Dex as interfacial passivator, b) UPS curves of neat ZnO and Dex-modified ZnO electrodes, c) conductivity curves of devices without and with the Dex modification, and d) transmittance curves of electrodes.

Among the newly developed methodologies, the fabrication of inverted OSCs (i-OSCs) is an effective way to achieve stable OSCs. In i-OSCs, the device architecture is typically ITO/electron transport layer (ETL)/active layer/HTL/anode,[14] where the ETL is usually fabricated using metal oxides and organic materials.[15] Although organics have been utilized as ETL in i-OSCs, disadvantages such as low conductivity and low electron mobility still exist, which hinder their wide application as efficient ETLs. Consequently, semiconducting metal oxides, such as ZnO,[16–20] $SnO_2$,[21,22] and $TiO_2$,[23,24] have become the most promising candidates as ETLs in i-OSCs. Among these metal oxides, ZnO is one of the most utilized ETLs in i-OSCs owing to its feasible solution processability in the sol-gel method, suitable energy-level alignment, high conductivity, and high electron mobility. Although ZnO is widely used as an ETL in i-OSCs, it has difficulties in realizing high performance and stable photovoltaic properties. For instance, the ZnO layer in i-OSCs processed through the sol-gel method exhibits distinct defects at the interface, where high-temperature processing (≈250 °C) for heating the ZnO gel to obtain the ETL layer forms oxygen valance and dangling bonds, which are potential charge carrier recombination centers, which causes low photovoltaic performance.[25,26] To address these problems in ZnO ETL, some useful strategies for interfacial modification have been explored, such as the introduction of organic and polymeric interfacial materials on top of the ZnO layer,[27,28] using boric acid to remove the hazardous amine additive in the sol-gel ZnO ETL,[29] and developing a conjugated molecule/ZnO hybrid layer.[30,31] Although these strategies can modify and improve the ZnO layer interface, most are chemically synthesized at a high cost. As OPVs are recognized as environmentally friendly and sustainable technologies, developing a green and effective interfacial engineering method to optimize the ZnO ETL in i-OSCs is necessary.

As mentioned previously, the interfacial layer is crucial for passivating and optimizing the ZnO layer. To overcome the drawbacks of recently synthesized interfacial layers with high cost and environmental unfriendliness, green and natural eco-friendly products with low cost have been used as efficient interfacial passivators to modify the ZnO layers in i-OSCs. Dextran (Dex; the chemical structure is displayed in **Figure 1**), as one of the natural products, is widely used in food and medical science, ascribing to its merits in non-toxicity and excellent biocompatibility, which demonstrates that Dex is a very green and environmentally friendly material.[32,33] Furthermore, compared to other natural products such as chitosan and cellulose, Dex demonstrates high solubility in green solvents without the need for chemical functionalization, which is beneficial for solution-processable techniques in OSCs. Additionally, specific groups in Dex, such as hydroxyl and ether groups, can interact with ZnO through hydrogen bonding and coordination, reducing defects caused by dangling bonds and oxygen vacancies, thereby resulting in efficient interfacial passivation. Owing to these advantages, Dex can potentially play an important role as an interfacial layer in i-OSCs. In this study, Dex was utilized as an interfacial passivator to modify the ZnO ETL and realize high-efficiency i-OSCs. Introducing a Dex layer was found to effectively modify the surface of the ZnO layer with decreased work function (*WF*) as well as enhanced conductivity. Interestingly, the Dex-modified ZnO layer as an ETL exhibited general applicability in i-OSCs with different active layers, including polymer:fullerene, polymer:nonfullerene, and all-polymer systems. Owing to the introduction of the Dex layer, these three types of i-OSCs demonstrated higher

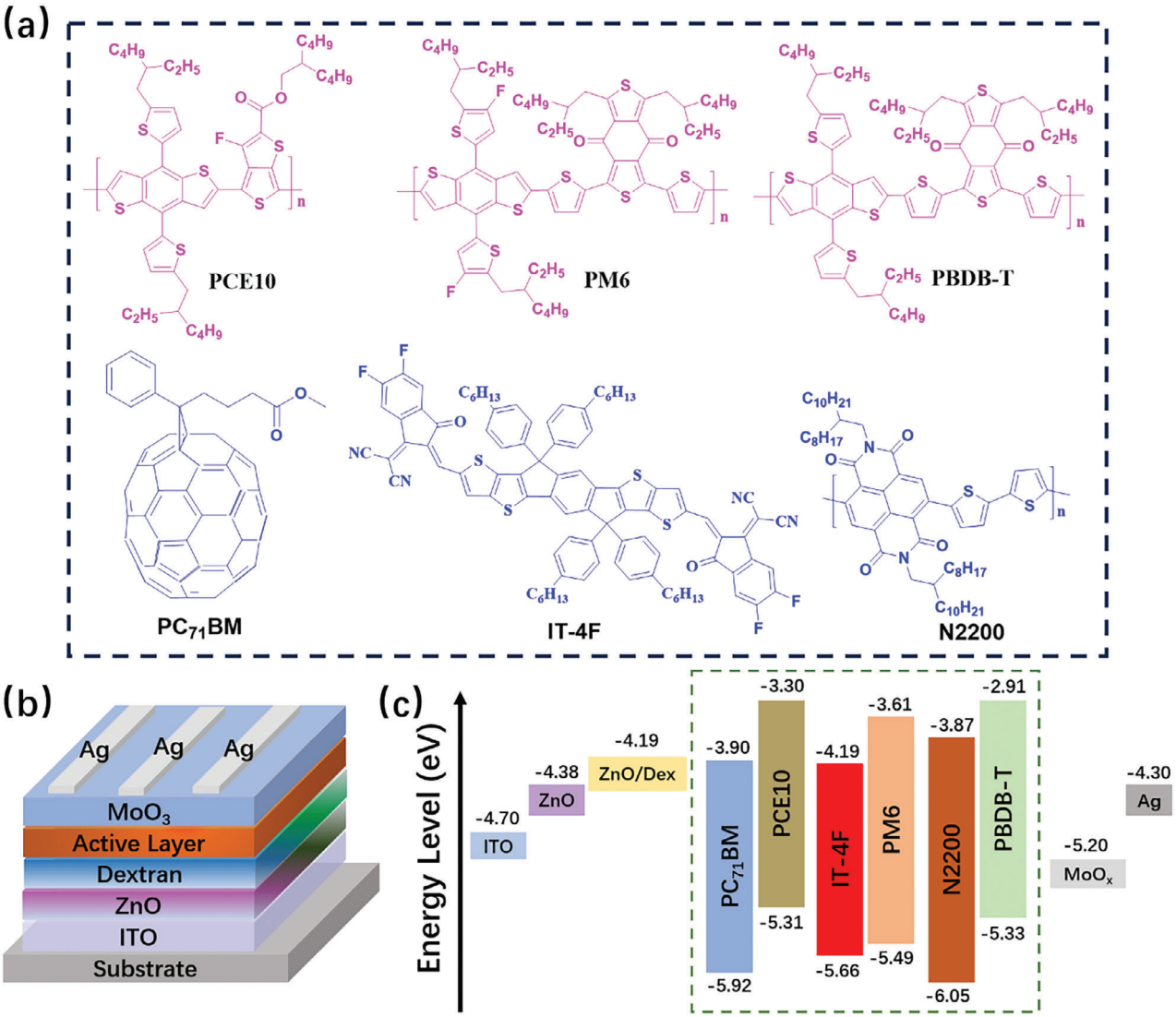


**Figure 2.** a) Chemical structures of active layers, b) device structure, and c) energy level diagram in i-OSCs.

photovoltaic performances by suppressing interfacial recombination and energy loss. To further explore the universal application of Dex-passivated ZnO as an ETL, three other types of non-fullerene OSCs were used to evaluate the interfacial function of Dex: PM6:Y6, D18:Y6, and PM6:PY-IT. The photovoltaic performances of all these systems can be efficiently improved by Dex modification, accompanied by enhanced stability. In particular, the D18:Y6 system yielded the highest PCE of 18.32% for i-OSCs when using Dex as the interfacial layer. Therefore, the natural product Dex shows an outstanding capability for passivating ZnO as an ETL for the pursuit of high-performance and stable i-OSCs.

## 2. Results and Discussion

### 2.1. Interfacial Passivation and Work Mechanism

It has been established that surface defects can form during the sol-gel process used to prepare ZnO ETLs, which significantly impair the photovoltaic performance of i-OSCs. As illustrated in Figure 1a, high-temperature processing can induce interfacial defects, particularly oxygen vacancies, resulting in exposed Zn-pendant bonds. These defects lead to elevated interfacial recombination in i-OSCs. When Dex is applied to the surface of the ZnO layer, the oxygen atom in the ether bond of Dex coordinates with the exposed Zn ions to form a favorable interfacial passivating bond (passivator), which decreases the interfacial defects in the ZnO layer and reduces the interfacial recombination. Furthermore, the hydroxyl group in Dex can form hydrogen bonds with the oxygen in the ZnO matrix, further diminishing the interfacial defects. To further verify the interfacial interactions between Dex and ZnO, Fourier transform infrared spectroscopy (FTIR) was performed, as shown in Figure S1 (Supporting Information). Notably, the absorption peak at 3414 $cm^{-1}$ is denoted as the -OH vibration in Dex. However, this absorption peak broadened and shifted to 3344 $cm^{-1}$ in the ZnO/Dex composite, which indicates that an interfacial hydrogen bond was possibly formed

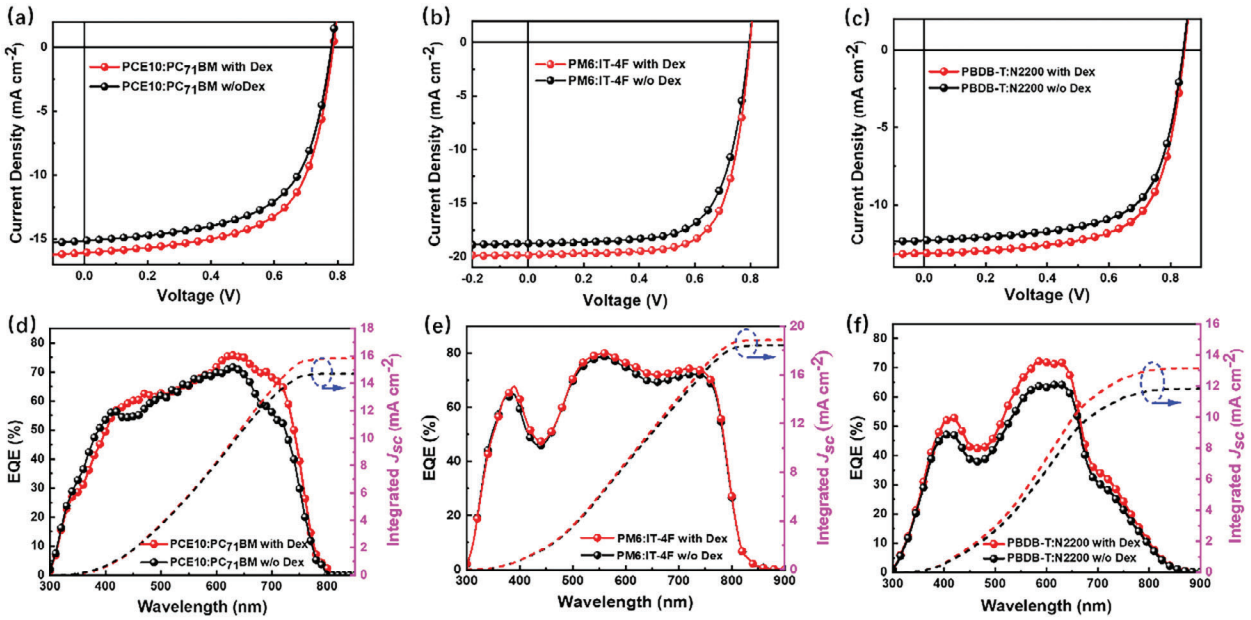


**Figure 3.** *J-V* and EQE characterization. *J-V* curves (a-c): a) for PCE10:$PC_{71}$BM, b) for PM6:IT-4F, and c) for PBDB-T:N2200; and EQE curves (d-f): d) for PCE10:$PC_{71}$BM, e) for PM6:IT-4F, and f) for PBDB-T:N2200.

between Dex and ZnO.[20,29,34] Furthermore, the absorption peak at 1159 $cm^{-1}$ was attributed to the C-O-C vibration in pristine Dex, whereas it shifted to 1155 $cm^{-1}$ when Dex was composited with the ZnO layer. This implies that the ether group interacted with the Zn ion and formed a weak interfacial coordination effect, which is a possible reason for passivation. To determine the effect of Dex on the *WF* of the ZnO layer, UV photoelectron spectroscopy (UPS) measurements were performed for the original ZnO film and the ZnO/Dex composite film, and the related curves are shown in Figure 1b.[35] The *WF* value of the original ZnO calculated based on the high binding energy cutoff was 4.38 eV, while ZnO/Dex had a lower *WF* of 4.19 eV. This result indicates that the Dex film on the ZnO layer helped reduce the energy barrier between ZnO and the active layer, which resulted in the formation of a good Ohmic contact between the active and composite interfacial layers, thereby facilitating charge transport between the active layer and the composite ETL. This is also supported by the increased conductive capability of the ZnO/Dex composite film compared to that of the bare ZnO film, as shown in Figure 1c and Figure S2 (Supporting Information). To investigate the effect of the Dex layer on the transparency of the ITO/ZnO composite films, the transmission spectra of ITO, ITO/ZnO, and ITO/ZnO/Dex were measured (Figure 1d). The introduction of the Dex layer did not affect the transmittance of the ITO/ZnO layer, which demonstrated corresponding average visible transmittance (AVT) values of 80.5% and 80.3% for the ITO/ZnO and ITO/ZnO/Dex ETLs, respectively, indicating that Dex did not affect light transmission to the active layer.

### 2.2. Photovoltaic Performance

As mentioned previously, the introduction of a Dex layer onto ZnO can affect the quality of the interfacial layer positively. OSCs were fabricated to evaluate the function of the Dex layer with an inverted device structure of ITO/ZnO (or ZnO/Dex)/active layer/$MoO_3$/Ag. To study the interfacial interactions with the active layers, three types of active materials were used: PCE10:$PC_{71}$BM for the fullerene system, PM6:IT-4F for the nonfullerene system, and PBDB-T:N2200 for all-polymer solar cells (all-PSCs). Their chemical structures, device architectures, and energy levels are shown in **Figure 2**. The effect of different Dex thicknesses on the photovoltaic performance was investigated by varying the concentration of the aqueous Dex solution during spin-coating on the ZnO layer, where PCE10:$PC_{71}$BM was used as the active layer. It was determined that the best concentration was 0.5 mg $mL^{-1}$ for obtaining the best photovoltaic performance, and the related *J-V* and EQE curves are presented in Figure S3 (Supporting Information) with the device performance summarized in Table S1 (Supporting Information).

As presented in **Figure 3**a–c, all devices based on different active layers with Dex modification displayed higher photovoltaic performance than the devices without Dex layers. Notably, no change was observed in the open-circuit voltage $V_{OC}$s; however, the short-circuit current density $J_{SC}$s increased obviously from 15.09 to 16.03, from 18.75 to 19.84, and from 12.27 to 13.12 mA $cm^{-2}$ for the PCE10:$PC_{71}$BM, PM6:IT-4F, and PBDB-T:N2200 systems, respectively. This increment in $J_{SC}$s is consistent with the results from the EQEs (Figure 3d–f), in which the photo-to-current efficiencies were distinctly enhanced when Dex layers were inserted between ZnO and the active layer. Furthermore, the FF values improved after introducing the Dex layer, and ultimately, the PCEs increased from 7.21% to 7.89%, from 10.31% to 11.04%, and from 6.85% to 7.41% for the PCE10:$PC_{71}$BM, PM6:IT-4F, and PBDB-T:N2200 systems (**Table 1**), respectively. These results indicate that natural Dex can function as an efficient interfacial passivator for ZnO as an ETL in i-OSCs.

**Table 1.** Summary of photovoltaic properties based on the devices without and with Dex modification under AM 1.5 G, 100 mw $cm^{-2}$.

| Active layer | Dex | $V_{OC}$ [V] | $J_{SC}$ [mA $cm^{-2}$] | $J^{b)}_{SC}$ [mA $cm^{-2}$] | FF [%] | PCE$^{a)}_{avg}$ [%] | $PCE_{max}$ [%] |
|---|---|---|---|---|---|---|---|
| PCE10: $PC_{71}BM$ | w/o | 0.78 | 15.09 | 14.70 | 61.35 | 7.07(±0.14) | 7.21 |
| | with | 0.78 | 16.03 | 15.81 | 63.11 | 7.76(±0.13) | 7.89 |
| PM6: IT-4F | w/o | 0.80 | 18.75 | 18.44 | 68.29 | 10.05 (±0.09) | 10.19 |
| | with | 0.80 | 19.84 | 18.89 | 71.11 | 11.02 (±0.17) | 11.26 |
| PBDB-T:N2200 | w/o | 0.84 | 12.27 | 11.82 | 66.41 | 6.70(±0.15) | 6.85 |
| | with | 0.84 | 13.12 | 13.11 | 67.21 | 7.31(±0.10) | 7.41 |

[a)] average PCE values from ten individual devices; [b)] $J_{SC}$ calculated from the integration of the EQE curves.

### 2.3. Interfacial Morphology Investigation

To investigate the effects of Dex on the surface properties of the ZnO ETLs, the water contact angles of the ZnO films were measured before and after Dex modification, as shown in **Figure** 4a,d. The water contact angle of pristine ZnO without Dex was 62°, indicating that an excessive contact angle was not conducive to surface wetting. However, the surface energy of the ZnO film after Dex modification was significantly reduced, and its water contact angle was reduced to 29°, which indicates that the ZnO surface was effectively covered and modified by Dex.

To further explore the surface properties, the surface morphologies with different ETLs were measured using atomic force microscopy (AFM), as shown in Figure 4b,c,e,f, where Figure 4b,e are height maps and Figure 4c,f are 3D spatial maps for pristine ZnO and Dex-modified ZnO films, respectively. Owing to the fine preparation process of the sol-gel ZnO film, the surface of the obtained pristine ZnO film was relatively smooth, with a surface roughness (RMS) of 2.48 nm. When the ZnO layer was modified by Dex, the RMS became 2.52 nm with almost no change compared to the ZnO film. This is probably because the upper Dex layer in the ZnO/Dex composite film was relatively thin, resulting in insignificant changes in the surface roughness of the composite ETLs. Furthermore, the very low RMS values of both the bare and Dex-covered ZnO layers are beneficial for casting the active layer to form a uniform film.

To further understand the surface details of ZnO/Dex composite interface, X-ray photoelectron spectroscopy (XPS) was

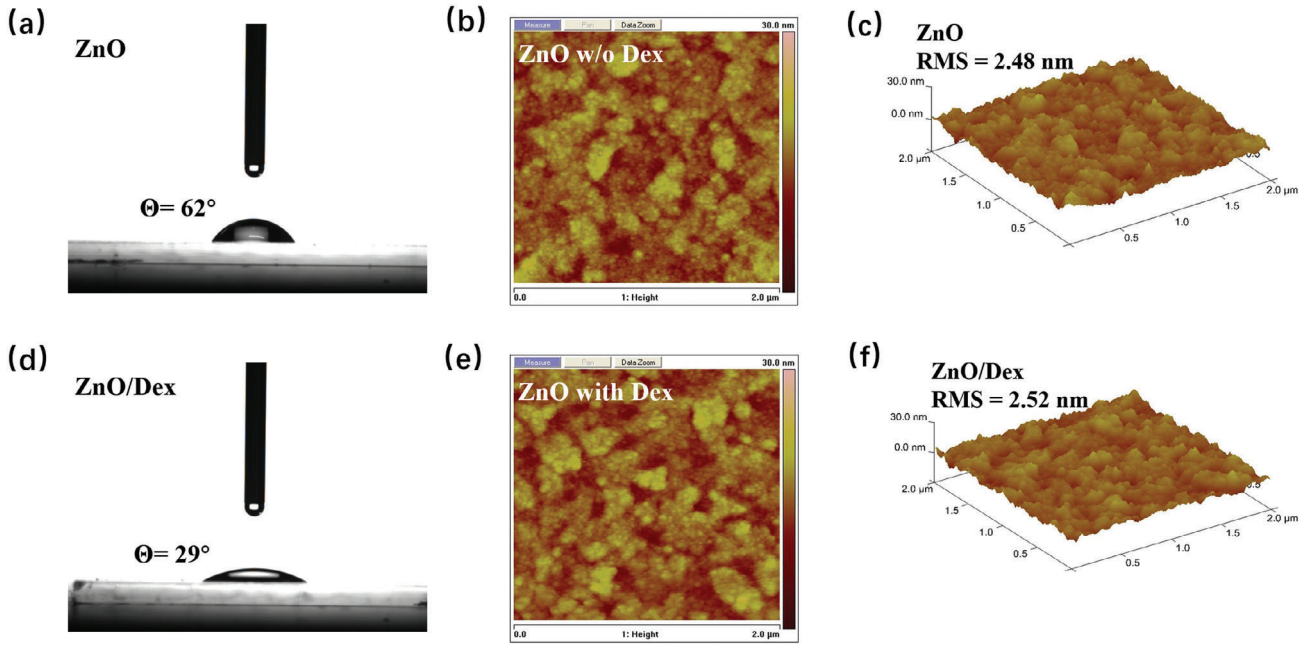


**Figure 4.** Water contact angle and AFM images (size: 2 μm × 2 μm) of: a,d) water contact angle images, b,e) 2D AFM images, and c,f) 3D AFM images for ZnO and Dex-decorated ZnO layers.

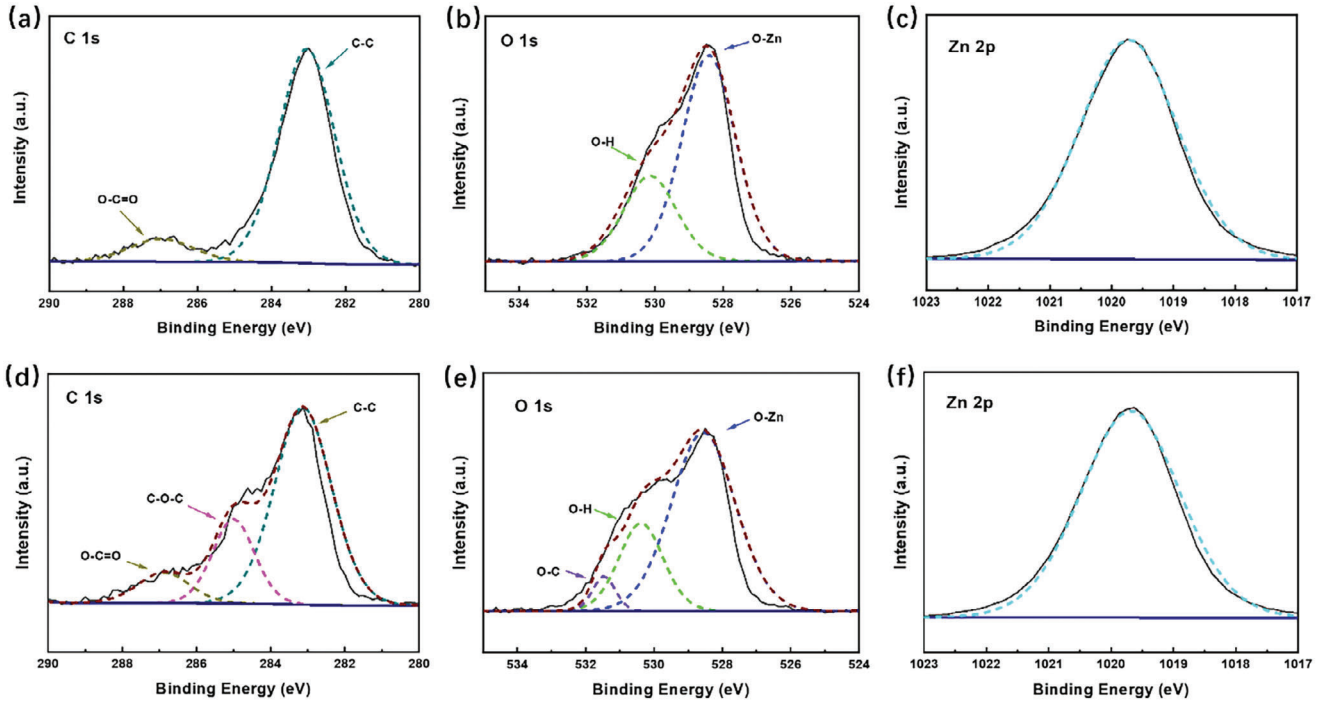


**Figure 5.** XPS spectra of: a,d) C 1s, b,e) O 1s, and c,f) Zn 2p for ZnO and Dex-decorated ZnO layers.

utilized to evaluate the ETLs, as shown in **Figure 5** (the XPS full spectra were presented in Figure S4, Supporting Information). Figure 5a,d shows the C1s signals of the pristine and Dex-covered ZnO ETLs, respectively. The pristine ZnO film exhibits two obvious peaks at binding energies of 283.1 and 287 eV, corresponding to the -C-C and carboxyl bonds, respectively. The -C-C bond in pristine ZnO mainly originates from the ethanolamine stabilizer when preparing the sol-gel ZnO film and the by-product of thermal annealing at high temperatures, while the carboxyl bonds possibly originate from the carboxylate salts of the reactant and intermediate product through thermal hydrolysis. In contrast to pristine ZnO, the Dex-covered ZnO exhibited an extra shoulder peak at 285 eV, as shown in Figure 5d, which indicates the existence of a C-O-C bond. This shoulder peak demonstrates that the Dex film was perfectly deposited on the ZnO. The O1s spectra of the pristine and Dex-deposited ZnO films are shown in Figure 5b,e, respectively. As shown in Figure 5b, it exhibited a typical asymmetric shape for O1s spectra. The lower binding energy (528.5 eV) corresponds to the O-Zn bond from the ZnO matrix, whereas the higher shoulder-binding energy at 530.1 eV is ascribed to the oxygen-deficient component (such as the zinc hydroxide bond). Compared to pristine ZnO, the composite ETL deposited by Dex exhibited stronger signals at higher binding energies of 530.4 and 531.5 eV, which were mainly attributed to the -OH and C-O bonds in Dex, respectively. In particular, the binding energy of hydroxyl in the Dex-covered ZnO was 0.3 eV higher than that of the pristine ZnO film, which indicates that the oxygen-deficient state is effectively passivated by Dex, similar to the evidence that appeared in the FTIR test results. Figure 5c,f shows that the Zn2p binding energy spectra peaked at 1019.8 eV for both the pristine ZnO and Dex-deposited composite films without prominent differences. Through contact angle, AFM, and XPS analyses, it was demonstrated that Dex can adhere to the ZnO interface effectively, which is beneficial for passivating interfacial defects and improving the photovoltaic performance of i-OSCs.

### 2.4. Charge Carrier Transport and Recombination Dynamics

To explore the interfacial charge transport properties, *J-V* curves were measured in the dark, as shown in Figure S5 (Supporting Information). The Dex-modified devices exhibited a reduced reverse saturation current density, implying better charge transport ability than the devices without the Dex layer. To further identify the interfacial electron transport, the space-charge-limited current (SCLC) method was employed to measure the electron mobilities of the active layers, where the electron-only devices followed the device structure of ITO/ZnO/with or without Dex/active layer/PDINN/Ag. As shown in Figure S6 (Supporting Information), the devices without Dex demonstrated electron mobilities of $1.98 \times 10^{-4}$, $2.90 \times 10^{-4}$, and $1.78 \times 10^{-4}$ $cm^2\ V^{-1}\ s^{-1}$ for the PCE10:$PC_{71}$BM, PM6:IT-4F, and PBDB-T:N2200 systems, respectively, while the values were improved to $2.72 \times 10^{-4}$, $4.52 \times 10^{-4}$, and $4.64 \times 10^{-4}$ $cm^2\ V^{-1}\ s^{-1}$ for the PCE10:$PC_{71}$BM, PM6:IT-4F, and PBDB-T:N2200 systems, respectively. Both reduced reverse saturation current densities and improved electron mobilities in Dex-modified devices demonstrate enhanced charge transport abilities, accounting for the increased $J_{SC}$ values of the corresponding i-OSCs with the Dex layer.[36] Furthermore, the relationship between the photogenerated current density ($J_{ph}$) and effective voltage ($V_{eff}$) was studied in detail to determine the corresponding charge dissociation rate, as displayed in Figure S7 (Supporting Information). The photogenerated current densities

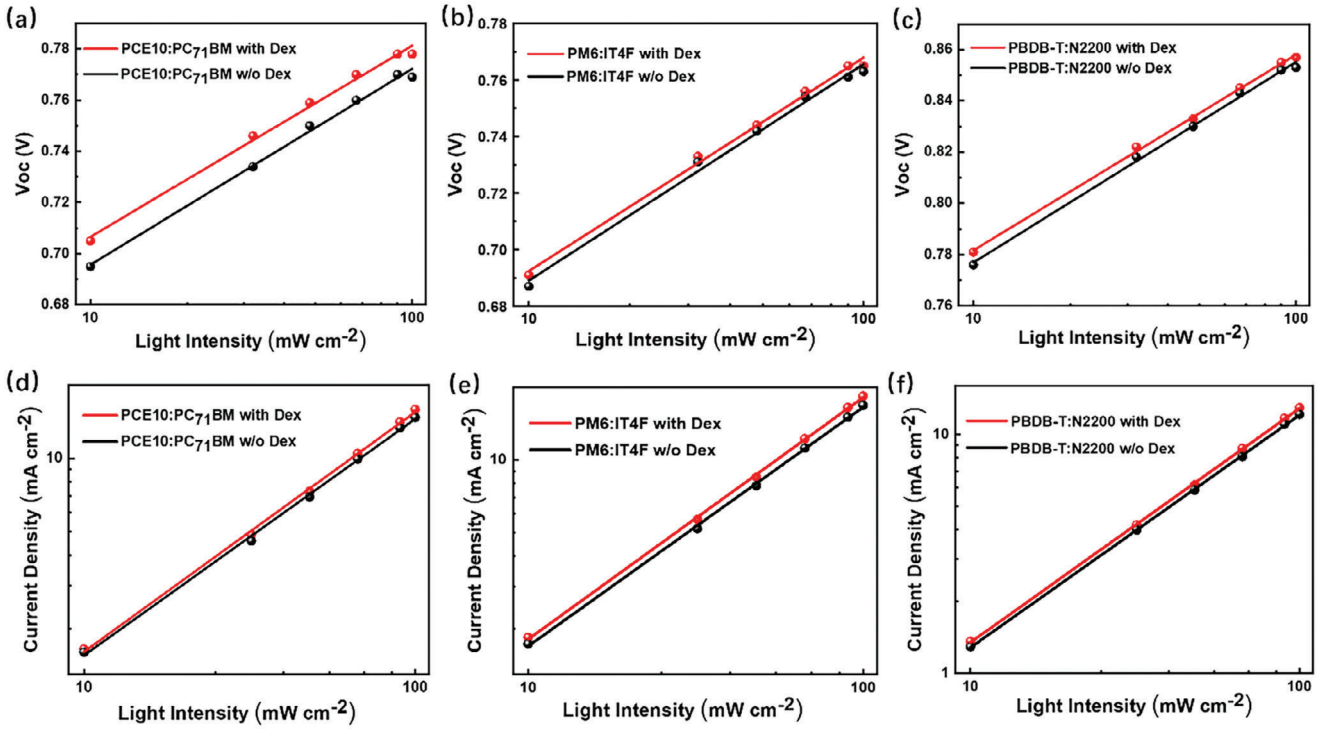


**Figure 6.** Charge carrier dynamics test for the $V_{OC}$-light intensity (ln I) characteristics (a-c): a) for PCE10:$PC_{71}BM$, b) for PM6:IT-4F, and c) for PBDB-T:N2200, respectively; and $J_{SC}$-light Intensity characteristics (d-f): d) for PCE10:$PC_{71}BM$, e) for PM6:IT-4F, and f) for PBDB-T:N2200.

of all the devices reached saturation ($J_{sat}$) at high $V_{eff}$, which indicates complete exciton dissociation and collection, respectively. Exciton dissociation rates ($\eta_{diss} = J_{ph}{}^{SC}/J_{sat}$) of 94.9%, 94.6%, and 93.3% were obtained for the PCE10:$PC_{71}BM$, PM6:IT-4F, and PBDB-T:N2200 systems without the Dex layer, respectively. When Dex was introduced as the passivator, the values of $\eta_{diss}$ improved to 96.1%, 97.2%, and 95.3% for the PCE10:$PC_{71}BM$, PM6:IT-4F, and PBDB-T:N2200 systems, respectively. This result indicates that the introduction of Dex on the ZnO layer enhanced the exciton dissociation capabilities of i-OSCs, resulting in higher FFs and $J_{SC}$s.

It has been established that the interfacial modification of ETLs in OSCs efficiently improves the photovoltaic performance by reducing the charge carrier recombination at the interfaces. In this study, the light intensity dependence of $V_{OC}$s and $J_{SC}$s was investigated to study the bimolecular recombination dynamics in Dex-modified i-OSCs.[37,38] The linear curves of the $V_{OC}$s-light intensity relationship are shown in **Figure** 6a–c, in which the linear correlation is obeyed by the formula rule of $V_{OC} \propto nkTln(I)/q$ (in this formula, the relative parameters of q, I, T, and k are elementary charge, light intensity, the Kelvin temperature, and the Boltzmann constant, respectively). The slopes of the devices for PCE10:$PC_{71}BM$, PM6:IT-4F, and PBDB-T:N2200 without Dex modification were 1.279, 1.277, and 1.303 kT $q^{-1}$, respectively, whereas those of the devices with Dex modification were 1.248, 1.259, and 1.275 kT $q^{-1}$, respectively. It is clear that the Dex-modified devices exhibited lower slopes than the devices with pristine ZnO as the ETLs. This reduction implies that the introduction of Dex on the ZnO layer could decrease the interfacial trap-involved recombination and improve charge carrier transport and collection at the interface.[39] Furthermore, to explore the influence of bimolecular recombination, the measurement of $J_{SC}$ versus light intensity was performed, in which the relationship rule obeyed the formula of $J_{SC} \propto I^{\alpha}$, as shown in Figure 6d–f. It is widely known that the bimolecular recombination would be minimized when the value of $\alpha$ is very close to 1. As presented in Figure 6d–f, the fitted $\alpha$ values were tracked as 0.969, 0.989, and 0.974 for the devices of PCE10:$PC_{71}BM$, PM6:IT-4F, and PBDB-T:N2200 without Dex modification, respectively. However, when Dex is introduced atop the ZnO layer, the $\alpha$ values improved to 0.984, 0.998, and 0.981 for PCE10:$PC_{71}BM$, PM6:IT-4F, and PBDB-T:N2200, respectively. By comparison with the devices without Dex modification, the $\alpha$ values of devices with the Dex-deposited ZnO layer were much closer to 1, which implies that the Dex-passivated ZnO layer could minimize the bimolecular recombination distinctly. Moreover, to further investigate the charge-carrier recombination effect, the trap-state density in the i-OSCs was calculated quantitatively by fabricating electron-only devices with the structure of ITO/ZnO/with or without Dex/active layer/PDINN/Ag, as presented in Figure S8 (Supporting Information). It shows that the trap-filled limited voltages ($V_{TFL}$s) for the devices without the Dex layer are 0.241, 0.166, and 0.186 V for PCE10:$PC_{71}BM$, PM6:IT-4F, and PBDB-T:N2200, respectively, corresponding to the related trap densities ($n_t$s) of $8.00 \times 10^{15}$, $5.51 \times 10^{15}$, and $6.17 \times 10^{15}$ $cm^{-3}$, respectively. When Dex was introduced as a passivating layer, the $V_{TFL}$s were reduced to 0.137, 0.097, and 0.108 V for PCE10:$PC_{71}BM$, PM6:IT-4F, and PBDB-T:N2200, respectively, corresponding to decreased $n_t$s of $4.55 \times 10^{15}$, $3.22 \times 10^{15}$, and $3.58 \times 10^{15}$ $cm^{-3}$, respectively. This distinct reduction in $n_t$s for the Dex-modified i-OSCs suggests

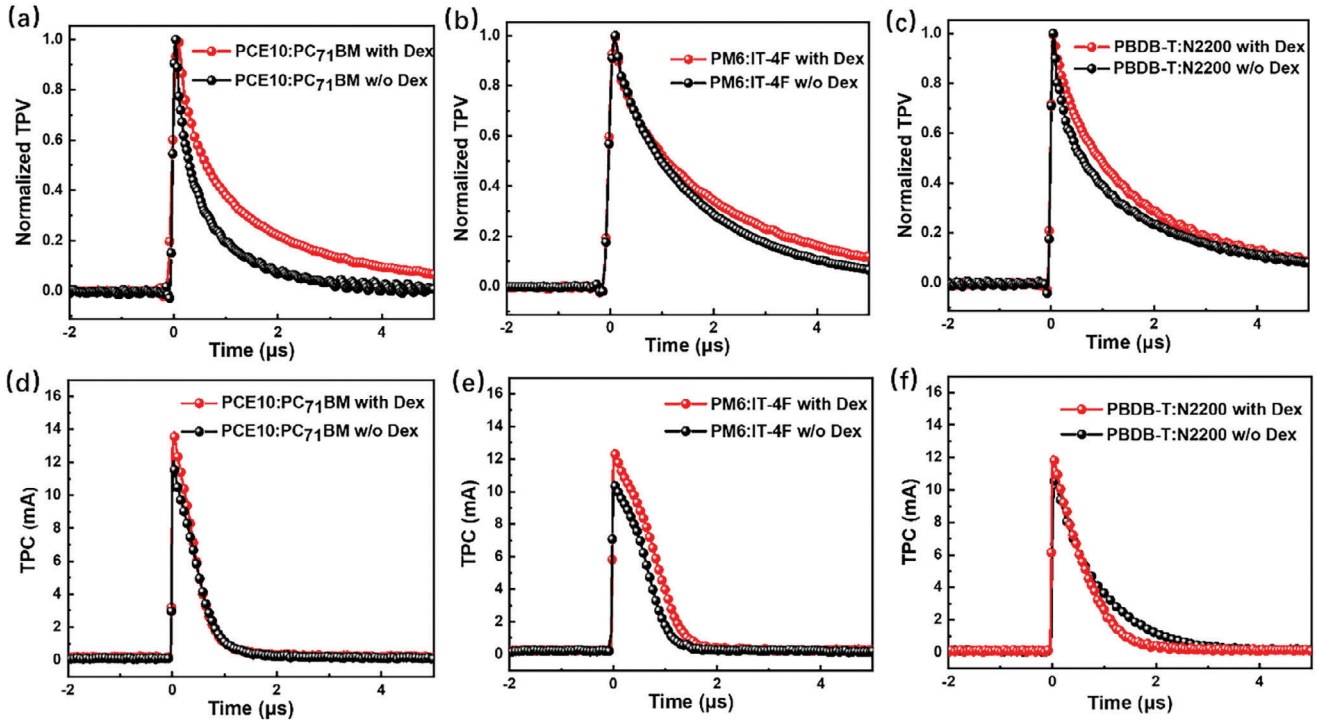


**Figure 7.** Charge carrier dynamics test for TPV-time characteristics (a-c): a) for PCE10:$PC_{71}$BM, b) for PM6:IT-4F, and c) for PBDB-T:N2200; and TPC-time characteristics (d-f): d) for PCE10:$PC_{71}$BM, e) for PM6:IT-4F, and f) for PBDB-T:N2200.

that Dex can efficiently passivate interfacial traps, and thereby inhibit interfacial recombination.[40] These results indicate that the deposition of Dex can reduce both trap-assisted and bimolecular recombination and enable efficient dissociation and extraction of charge carriers and their final collection by the electrodes.[41]

To study the charge carrier dynamics, transient photovoltage (TPV) and transient photocurrent (TPC) tests were performed, as shown in **Figure 7**.[42–44] For the TPV test, as shown in Figure 7a–c, the measured charge recombination decay lifetimes of PCE10:$PC_{71}$BM, PM6:IT-4F, and PBDB-T:N2200 without Dex modification were 0.59, 1.65, and 1.08 μs, respectively. After the introduction of Dex as a passivator on ZnO, the charge recombination decay lifetimes were lifted to 1.28, 2.01, and 1.35 μs for the PCE10:$PC_{71}$BM, PM6:IT-4F, and PBDB-T:N2200 systems, respectively. These extended charge recombination decay lifetimes indicate that the Dex layer can efficiently suppress interfacial charge recombination, which is beneficial for achieving high-performance OSCs.[45] Moreover, TPC was performed under the same test conditions. Through the integrated calculation, the extracted charge carriers under the short-circuit state were $6.26 \times 10^{-9}$, $7.26 \times 10^{-9}$, and $8.0 \times 10^{-9}$ C for the PCE10:$PC_{71}$BM, PM6:IT-4F, and PBDB-T:N2200 systems without Dex modification, respectively, while the amount of extracted charge carriers improved to $6.71 \times 10^{-9}$, $9.8 \times 10^{-9}$, and $9.45 \times 10^{-9}$ C for the PCE10:$PC_{71}$BM, PM6:IT-4F, and PBDB-T:N2200 systems with Dex modification, respectively. This improvement implies that the introduction of Dex could facilitate faster charge carrier extraction than without Dex modification, possibly because of better interfacial contact and greater passivation of the ZnO layer.[46] Overall, it is clear that the inserted Dex layer on the ZnO could decrease the interfacial bimolecular recombination and promote charge carrier extraction efficiently, which would sufficiently enhance the photovoltaic performance, including the $J_{SC}$s, FFs, and PCEs. Certainly, these excellent charge extraction processes under Dex modification are reflected by the above results of the high performance of inverted fullerene, non-fullerene, and all-polymer OSCs.

### 2.5. Broad Applications of Dex as Interfacial Passivator in i-OSCs

To further demonstrate the general applicability of Dex as an efficient interfacial passivator in i-OSCs, three other high-performance active layers were utilized in fabricating i-OSCs, including the non-fullerene systems of PM6:Y6 and D18:Y6 and an all-polymer system of PM6:PY-IT. The *J-V* and EQE curves are presented in **Figure 8**a–f and **Table 2**, respectively. The chemical structures of the active layers are shown in Figure S9 (Supporting Information). Notably, the photovoltaic performance of these three systems was improved when Dex was used as an interfacial passivator, where the D18:Y6-based OSC presented the highest PCE of 18.32%. To the best of our knowledge, this PCE is one of the highest values reported for binary i-OSCs (Figure S10 and Table S2, Supporting Information). To evaluate the improvement in stability achieved by Dex passivation, storage stability tests were performed, as shown in Figure 8g–i. Interestingly, all the devices with Dex passivation exhibited higher stabilities than those without the Dex layer and all exhibited excellent $T_{80}$ lifetimes of more than 1500 h. This improved stability of the devices with the Dex layer can be attributed to the suppressed interfacial

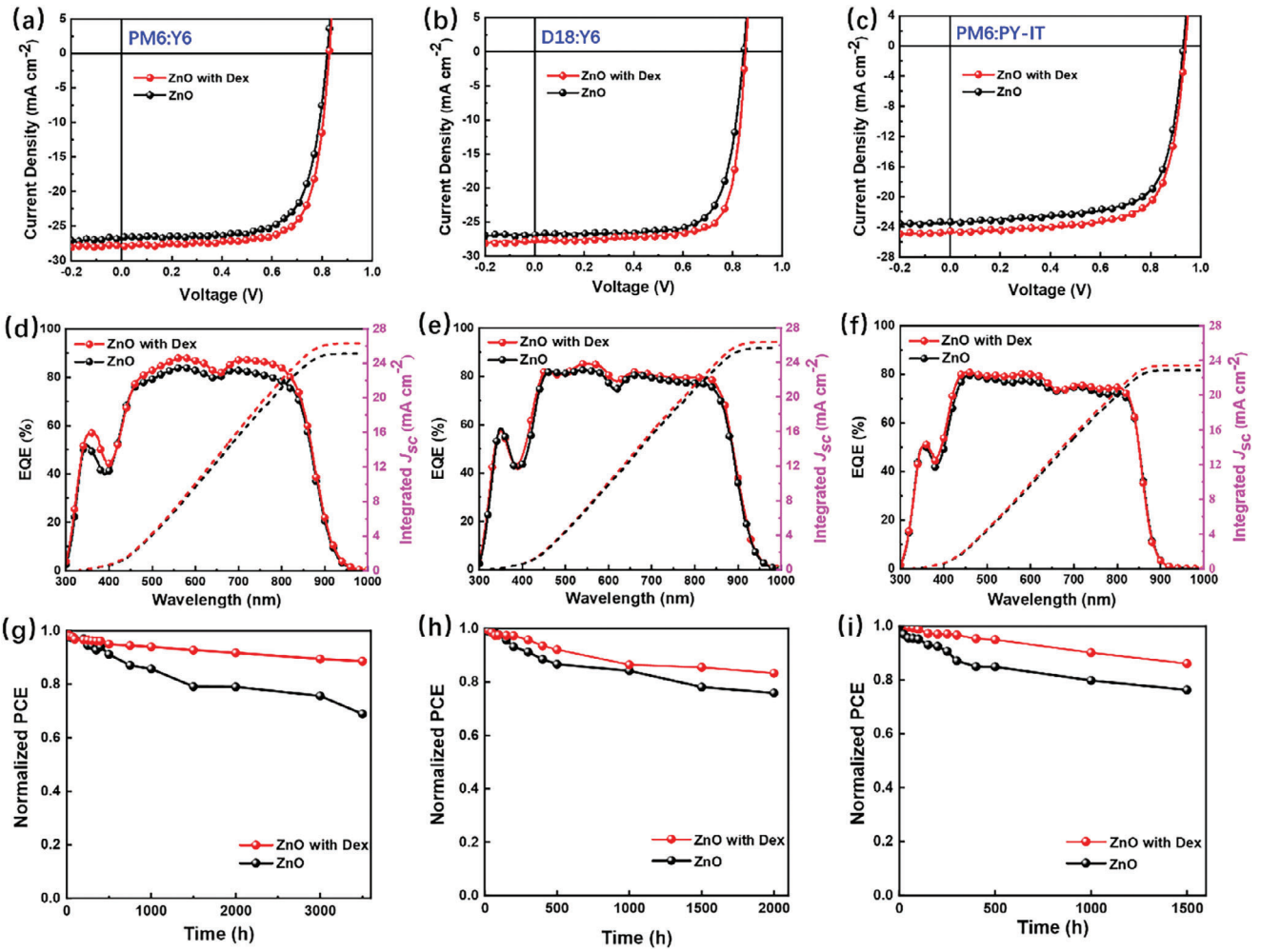


**Figure 8.** *J-V* and EQE characterization. *J-V* curves: a) for PM6:Y6, b) for D18:Y6, and c) for PM6:PY-IT; EQE curves (d-f): d) for PM6:Y6, e) for D18:Y6, and f) for PM6:PY-IT; and storage stability curves in $N_2$ glovebox at room temperature (g-i): g) for PM6:Y6, h) for D18:Y6, and (i) for PM6:PY-IT.

**Table 2.** Summary of the photovoltaic properties based on the devices without and with Dex modification under AM 1.5 G, 100 mW $cm^{-2}$.

| Active layer | Dex | $V_{OC}$ [V] | $J_{SC}$ [mA $cm^{-2}$] | $J^{b)}_{SC}$ [mA $cm^{-2}$] | FF [%] | PCE$^{a)}_{avg}$ [%] | $PCE_{max}$ [%] |
|---|---|---|---|---|---|---|---|
| PM6:Y6 | w/o | 0.82 | 26.73 | 25.70 | 71.42 | 15.32 (±0.20) | 15.66 |
| | with | 0.83 | 27.72 | 26.32 | 74.33 | 16.78 (±0.15) | 17.05 |
| D18:Y6 | w/o | 0.85 | 26.85 | 25.66 | 73.75 | 16.58 (±0.10) | 16.75 |
| | with | 0.85 | 27.68 | 26.38 | 77.52 | 18.02 (±0.19) | 18.32 |
| PM6: PY-IT | w/o | 0.93 | 23.35 | 22.87 | 71.36 | 15.23 (±0.20) | 15.53 |
| | with | 0.94 | 24.60 | 23.41 | 72.25 | 16.40 (±0.21) | 16.69 |

[a)] average PCE values from ten individual devices; [b)] $J_{SC}$ calculated from the integration of the EQE curves.

charge recombination and energy loss. To study the reproducibility of the device performance of the i-OSCs, statistical diagrams of the device performance were provided, as presented in Figure S11 (Supporting Information), which implies that all the devices exhibit good reproducibility in performance. These results indicate that Dex not only improves the PCE, but also enhances the stability, making it a potentially useful interfacial passivator for i-OSCs.

## 3. Conclusion

In conclusion, a natural and green product of Dex was used as an efficient interfacial passivator to passivate the defects of the ZnO ETL through interfacial O-Zn coordination and hydrogen bonding in i-OSCs. Through the introduction of the Dex layer, the *WF* of the ZnO layer reduced from 4.38 to 4.19 eV, efficiently lowering the electron transport barrier at the interface and improving the conductivity of the ZnO layer because of the decreased energy barrier. When Dex was used as an interfacial passivator in i-OSCs, interfacial recombination and energy loss were efficiently suppressed, which resulted in improved photovoltaic performance. Furthermore, Dex-passivated ZnO exhibited broad applications as an ETL in different types of i-OSCs, including fullerene (PCE10:$PC_{71}BM$), non-fullerene (PM6:IT-4F, PM6:Y6, and D18:Y6), and all-polymer (PBDB-T:N2200 and PM6:PY-IT) solar cells, where D18:Y6 demonstrated the highest PCE of 18.32%. Moreover, the application of Dex could efficiently improve the device stability, in which the $T_{80}$ lifetimes based on PM6:Y6, D18:Y6, and PM6:PY-IT exceeded 1500 h. Therefore, these results demonstrate that Dex is a useful and excellent interfacial passivator for ZnO as an ETL for high-performance i-OSCs. A detailed investigation of Dex showed that natural products are promising functional materials for OSCs, because they possess numerous different polar groups that might interact with metal electrodes and active layers efficiently. These findings encourage us to pay more attention to natural materials for their utilization in green and environmentally friendly organic photovoltaic technologies.

## 4. Experimental Section

The details of the materials, characterization, device fabrication, and tests are presented in the Supporting Information.

## Supporting Information

Supporting Information is available from the Wiley Online Library or from the author.

## Acknowledgements

This work was supported by the National Natural Science Foundation of China (52373175), the High-level Innovative Talents Foundation of Guizhou Province (QKHPTRC-GCC[2023]024), Natural Science Foundation of Guizhou Province (QKHPTRC-CXTD[2023]005), Science and Technology Innovation Team of Higher Education Department of Guizhou Province (QJJ[2023]053), Natural Science Foundation of Guizhou University (GZUTGH[2023]12), and Science and Technology Innovation Team of Guizhou University (GZUKCT[2023]01). E.W. thanks the Swedish Research Council (2019-04683, 2020–05223), Swedish Research Council Formas (2020-01201, 2023-01008), Swedish Energy Agency (P2021-90067), and the Wallenberg Foundation (2022.0192) for their financial support.

## Conflict of Interest

The authors declare no conflict of interest.

## Data Availability Statement

The data that support the findings of this study are available from the corresponding author upon reasonable request.

## Keywords

dextran, electron transport layers (ETLs), interfacial passivators, inverted organic solar cells (OSCs), zinc oxides

Received: September 19, 2024
Revised: December 22, 2024
Published online:

[1] P. Ding, D. Yang, S. Yang, Z. Ge, *Chem. Soc. Rev.* **2024**, *53*, 2350.
[2] Y. Sun, L. Wang, C. Guo, J. Xiao, C. Liu, C. Chen, W. Xia, Z. Gan, J. Cheng, J. Zhou, Z. Chen, J. Zhou, D. Liu, T. Wang, W. Li, *J. Am. Chem. Soc.* **2024**, *146*, 12011.
[3] Y. Jiang, S. Sun, R. Xu, F. Liu, X. Miao, G. Ran, K. Liu, Y. Yi, W. Zhang, X. Zhu, *Nat. Energy* **2024**, *9*, 975.
[4] Z. Zheng, J. Wang, P. Bi, J. Ren, Y. Wang, Y. Yang, X. Liu, S. Zhang, J. Hou, *Joule* **2022**, *6*, 171.
[5] L. Zhu, M. Zhang, J. Xu, C. Li, J. Yan, G. Zhou, W. Zhong, T. Hao, J. Song, X. Xue, Z. Zhou, R. Zeng, H. Zhu, C.-C. Chen, R. C. I. MacKenzie, Y. Zou, J. Nelson, Y. Zhang, Y. Sun, F. Liu, *Nat. Mater.* **2022**, *21*, 656.
[6] C. Guo, Y. Fu, D. Li, L. Wang, B. Zhou, C. Chen, J. Zhou, Y. Sun, Z. Gan, D. Liu, W. Li, T. Wang, *Adv. Mater.* **2023**, *35*, 2304921.
[7] M. Deng, X. Xu, Y. Duan, L. Yu, R. Li, Q. Peng, *Adv. Mater.* **2023**, *35*, 2210760.
[8] M. Lv, J. Huang, X. Luo, S. Yu, X. Wang, Z. Wang, F. Pan, B. Zhang, L. Ding, *Aggregate* **2024**, *5*, e544.
[9] Y. Tong, B. Xu, F. Ye, *Adv. Funct. Mater.* **2024**, *34*, 2310865.
[10] M.-F. Xu, X.-B. Shi, Z.-M. Jin, F.-S. Zu, Y. Liu, L. Zhang, Z.-K. Wang, L.-S. Liao, *ACS Appl. Mater. Interfaces* **2013**, *5*, 10866.
[11] J.-M. Wang, Z.-K. Wang, M. Li, K.-H. Hu, Y.-G. Yang, Y. Hu, X.-Y. Gao, L.-S. Liao, *ACS Appl. Mater. Interfaces* **2017**, *9*, 13240.
[12] C.-H. Hsieh, Y.-J. Cheng, P.-J. Li, C.-H. Chen, M. Dubosc, R.-M. Liang, C.-S. Hsu, *J. Am. Chem. Soc.* **2010**, *132*, 4887.
[13] X. Zhang, H. Zhang, Y. Li, S. Zafar, S. Yang, J. Chen, H. Zhou, Y. Zhang, *Adv. Funct. Mater.* **2022**, *32*, 2205398.
[14] Z. Yin, J. Wei, Q. Zheng, *Adv. Sci.* **2016**, *3*, 1500362.
[15] X. Li, W. Zhang, K. Usman, J. Fang, *Adv. Energy Mater.* **2018**, *8*, 1702730.
[16] Chambaili, I. A., K. Hayat, E. Ahmad, N. Ali, K. Safeen, A. Shah, V. Tirth, A. Algahtani, S. K. Shah, *Phys. Scr.* **2023**, *98*, 115962.
[17] A. Sreedharan, B. C. Das, *J. Phys. D: Appl. Phys.* **2022**, *55*, 335103.
[18] H. W. Lee, S. Biswas, H. Choi, Y. Lee, H. Kim, *Appl. Surf. Sci.* **2024**, *659*, 159930.
[19] H. Li, B. Yu, H. Yu, *Adv. Funct. Mater.* **2024**, *34*, 2402128.

[20] Z. Wang, Y. Ren, J. Meng, X. Zou, S. Wang, M. Zhao, H. Wang, Y. Hao, B. Xu, E. Wang, S. Yin, *J. Mater. Chem. A* **2023**, *11*, 1810.
[21] L. D. Mario, D. G. Romero, H. Wang, E. K. Tekelenburg, S. Meems, T. Zaharia, G. Portale, M. A. Loi, *Adv. Mater.* **2024**, *36*, 2301404.
[22] Y. Qiu, R. Peng, J. Shi, Z. Chen, Z. Ge, *Adv. Funct. Mater.* **2023**, *33*, 2300831.
[23] D.-H. Ko, J. R. Tumbleston, M.-R. Ok, H. Chun, R. Lopez, E. Samulski, *J. Appl. Phys.* **2010**, *108*, 083101.
[24] H. O. Seo, S.-Y. Park, W. H. Shim, K.-D. Kim, K. H. Lee, M. Y. Jo, J. H. Kim, E. Lee, D.-W. Kim, Y. D. Kim, D. C. Lim, *J. Phys. Chem. C* **2011**, *115*, 21517.
[25] O. Pachoumi, C. Li, Y. Vaynzof, K. K. Banger, H. Sirringhaus, *Adv. Energy Mater.* **2013**, *3*, 1428.
[26] R.-X. Ou, Y.-C. Chen, C.-H. Lin, T.-F. Guo, T.-C. Wen, *Org. Electron.* **2018**, *63*, 93.
[27] S. Li, Q. Fu, L. Meng, X. Wan, L. Ding, G. Lu, G. Lu, Z. Yao, C. Li, Y. Chen, *Angew. Chem., Int. Ed.* **2022**, *61*, e202207397.
[28] Y. Xin, H. Liu, X. Dong, Z. Xiao, R. Wang, Y. Gao, Y. Zou, B. Kan, X. Wan, Y. Liu, Y. Chen, *J. Am. Chem. Soc.* **2024**, *146*, 3363.
[29] Y. Wang, Z. Zheng, J. Wang, X. Liu, J. Ren, C. An, S. Zhang, J. Hou, *Adv. Mater.* **2023**, *35*, 2208305.
[30] L. Nian, W. Zhang, N. Zhu, L. Liu, Z. Xie, H. Wu, F. Würthner, Y. Ma, *J. Am. Chem. Soc.* **2015**, *137*, 6995.
[31] X. Wen, A. Nowak-Król, O. Nagler, F. Kraus, N. Zhu, N. Zheng, M. Müller, D. Schmidt, Z. Xie, F. Würthner, *Angew. Chem., Int. Ed.* **2019**, *58*, 13051.
[32] Z. Chen, J. Chen, D. Ni, W. Xu, W. Zhang, W. Mu, *Food Chem.* **2024**, *437*, 137951.
[33] M. S. Khan, B. H. J. Gowda, N. Nasir, S. Wahab, M. R. Pichika, A. Sahebkar, P. Kesharwani, *Int. J. Pharm.* **2023**, *643*, 123276.
[34] S. Zhou, X. Zheng, X. Yu, J. Wang, J. Weng, X. Li, B. Feng, M. Yin, *Chem. Mater.* **2007**, *19*, 247.
[35] B. Zhang, Y. Zhao, C. Xu, C. Feng, W. Li, X. Qin, M. Lv, X. Luo, X. Qin, A. Li, Z. He, E. Wang, *Adv. Funct. Mater.* **2024**, *34*, 2400903.
[36] M. Morsli, L. Cattin, J. C. Bernède, P. Kumar, S. Chand, *J. Phys. D: Appl. Phys.* **2010**, *43*, 335103.
[37] C. He, Y. Pan, Y. Ouyang, Q. Shen, Y. Gao, K. Yan, J. Fang, Y. Chen, C.-Q. Ma, J. Min, C. Zhang, L. Zuo, H. Chen, *Energy Environ. Sci.* **2022**, *15*, 2537.
[38] Q. Chen, H. Huang, D. Hu, C. Zhang, X. Xu, H. Lu, Y. Wu, C. Yang, Z. Bo, *Adv. Mater.* **2023**, *35*, 2211372.
[39] X. Wang, S. Yi, Z. He, X. Ouyang, H. Wu, W. Zhu, B. Zhang, Y. Cao, *Sustain. Energ. Fuels* **2020**, *4*, 1234.
[40] Z. Ge, J. Qiao, J. Song, X. Li, J. Fu, Z. Fu, J. Gao, X. Tang, L. Jiang, Z. Tang, G. Lu, X. Hao, Y. Sun, *Adv. Energy Mater.* **2024**, *14*, 2400203.
[41] S. Jeong, A. Rana, J.-H. Kim, D. Qian, K. Park, J.-H. Jang, J. Luke, S. Kwon, J. Kim, P. S. Tuladhar, J.-S. Kim, K. Lee, J. R. Durrant, H. Kang, *Adv. Sci.* **2023**, *10*, 2206802.
[42] R. C. I. MacKenzie, C. G. Shuttle, M. L. Chabinyc, J. Nelson, *Adv. Energy Mater.* **2012**, *2*, 662.
[43] R. A. Street, *Phys. Rev. B* **2011**, *84*, 075208.
[44] C. Sae-Kung, B. F. Wright, T. M. Clarke, G. G. Wallace, A. J. Mozer, *ACS Appl. Mater. Interfaces* **2019**, *11*, 21030.
[45] Z. Wu, C. Sun, S. Dong, X.-F. Jiang, S. Wu, H. Wu, H.-L. Yip, F. Huang, Y. Cao, *J. Am. Chem. Soc.* **2016**, *138*, 2004.
[46] G. Chen, G. Qian, S. Yi, Z. He, H.-B. Wu, W. Yang, B. Zhang, Y. Cao, *ACS Appl. Mater. Interfaces* **2019**, *11*, 45969.